Long-range hopping and indexing assumption in one-dimensional topological insulators

R. G. Dias* and A. M. Marques
Department of Physics & i3N, University of Aveiro, 3810-193 Aveiro, Portugal

(Received 19 September 2021; accepted 21 December 2021; published 3 January 2022)

In this paper, we show that the introduction of long-range hoppings in one-dimensional topological insulator models implies that different possibilities of site indexing must be considered when determining the bulk topological invariants in order to avoid the existence of hidden symmetries. The particular case of the extended Su-Schrieffer-Heeger chain is addressed as an example where such behavior occurs. In this model, the introduction of long-range hopping terms breaks the bipartite property and a band inversion occurs in the band structure as the relative values of the hopping terms change, signaling a crossover between hopping parameter regions of "influence" of different chiral symmetries. Furthermore, edge states become a linear combination of edgelike states with different localization lengths and reflect the gradual transition between these different chiral symmetries.

DOI: 10.1103/PhysRevB.105.035102

I. INTRODUCTION

Topological insulators (and superconductors) are categorized according to their dimension and to general symmetries that protect gapless boundary modes [1,2]. One of the latter is the chiral symmetry or sublattice symmetry which protects the zero energy edge states of bipartite lattices such as the Su-Schrieffer-Heeger (SSH) model due to the anticommutation of the chiral operator $\mathcal{C}$ (the difference of the projection operators in the two sublattices of the system) and the Hamiltonian. It is usual in the case of translational invariant Hamiltonians to assume that the latter is equivalent to the relation $\mathcal{C}H(k)\mathcal{C}^{-1} = -H(k)$, where implicitly a choice of unit cell has been undertaken. Furthermore, several topological invariants such as the Zak's phase [3] or the Chern number [4] rely on the knowledge of Bloch eigenstate $|u_{\pm}(k)\rangle$ throughout the Brillouin zone and also reflect a particular choice of unit cell. Each choice of unit cell implies a particular subdivision of the lattice into sublattices.

In this paper, we argue that, in the case of linear chains with long-range hoppings (beyond nearest neighbor and that may break the bipartite property), several choices of site indexing should be considered in order to correctly describe their bulk topological behavior, which correspond to *different representations of the tight-binding Hamiltonian as a linear chain*. If the indexing is not the "correct" one, the topological protection of edge states may be associated with a *hidden chiral symmetry* [5–9], which cannot be written as a difference of projection operators onto the sublattices defined by the unit cell. This will be expected in particular if a band inversion occurs in the band structure of the linear chain as the relative values of the hopping terms change. In order to illustrate the previous arguments, we consider in this paper the chiral symmetry protected topological SSH insulator and add to it long-range hopping terms [10–22] in such a way that the Hamiltonian eigenbasis remains the same and the usual SSH chiral operator remains a mapping operator between eigenstates of the Hamiltonian (allowing us to compare it with new chiral operators). This model is simply the extended SSH chain with next-nearest-neighbor (NNN) hoppings. For certain evolutions of the ratio between hopping parameters, a band inversion will occur signaling a crossover between parameter regions of "influence" of different chiral symmetries (regions where the Hamiltonian can be adiabatically changed in order to recover a chiral symmetry).

We also present an analytical and numerical study of the topological edge states of this extended SSH chain in the presence of open boundary conditions (OBC), and show that they reflect clearly the indexing problem and the existence of different chiral symmetries. The extended hopping terms imply that the edge states cannot be generated from degenerate bulk states and this leads to the existence of two localization lengths in the real-space dependence of the edge states. In a log plot, such behavior is clearly observed as well as the existence of competition between the different chiral symmetries in the edge state profile in the crossover region.

This paper is organized in the following way. In Sec. II, we introduce in general terms the indexing problem. In the next section, we construct the extended SSH model and discuss the indexing problem in this model. In Sec. IV, we address limiting cases of the extended SSH model where a chiral symmetry is present. In Sec. IV, we present a discussion of the edge states in this model. Finally we conclude.

II. INDEXING ASSUMPTION

Let us consider a linear chain with finite range extended hopping terms and a unit cell with n sites, where n is even. Instead of the shortest unit cell associated with the translational symmetry, we consider a larger unit cell with size at least large enough so that hopping terms within the unit cells

*rdias@ua.pt

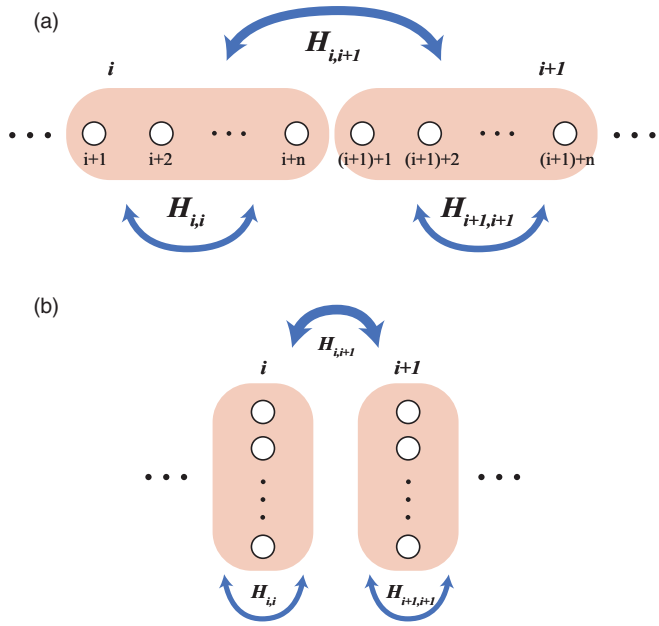

FIG. 1. (a) Linear chain with finite range extended hopping terms and a unit cell with n sites such that only hopping terms within the unit cells ($H_{i,i}$) or between consecutive unit cells ($H_{i,i+1}$) are present. (b) Reinterpretation of the linear chain as a ladder with a rung with n sites. Different indexings of the ladder sites generate different linear chains.

and between consecutive unit cells are present; see Fig. 1(a). This chain can be interpreted as a ladder with a rung of n sites as shown in Fig. 1(b). Our chain has n sublattices (all with the same cardinality) and the site j belongs to the sublattice $[(j+1)\mathrm{mod}\, n]-1$. If the ladder was our starting point, then the original linear chain would be obtained with a zig-zag indexing of the sites in the ladder shown in Fig. 1(b); that is, our linear chain constitutes a particular path in our ladder that generates a periodic sequence of nearest-neighbor (NN) hoppings as well as of the longer range hopping terms. The respective periodicity defines the unit cell of the linear chain and it should be obvious that an infinite number of different paths exist, but in general with larger unit cells.

Starting from a ladder and given some hopping terms distribution, it should be possible to find the path (or paths) corresponding to the shortest unit cell (which may be smaller than the number of sites in each rung). Given one of these paths, one can circularly permutate the indexing of sites in a given sublattice without increasing the unit cell, but at the cost of introducing longer range hopping terms in general. If we permutate in a noncircular way the sites in a given sublattice, the unit cell size will increase or one may even lose completely the translational invariance in the linear chain (but a hidden translational invariance will be present in the Hamiltonian). One would naturally assume that the indexing corresponding to the shortest unit cell would allow for the full topological characterization of the linear chain, but there is a subtle problem concerning the protecting symmetries of the edge states when our linear chain has long-range hopping that we explain in the following.

Given our ladder of n sites per rung, it is possible to change the hopping parameters so that a single path is present such that all sites are only connected to their nearest neighbors in the corresponding linear chain. This chain is bipartite (with the odd and even sublattices having the same cardinality) and therefore it has chiral symmetry reflecting the existence of hopping terms only between even and odd sublattices. One may ask how many different such chiral symmetries (as a simplification, we consider only the chiral symmetries reflecting a partition of the lattice into two sublattices with the same cardinality, but the argument can in principle be generalized to any ratio of the sublattice cardinalities) can be found given an n-site unit cell (the ladder rung) and allowing only changes in the magnitudes of the hopping terms (no on-site potentials are introduced). This can be answered considering the possible linear paths (with only nearest-neighbor hopping) that generate different sublattices. Note that these linear paths include a single hopping term between consecutive unit cells since we can do a circular permutation of indexing within the sublattices in order to ensure that. The number of different chiral symmetries is $n(n-1)/2$ and the simplest topological linear chain corresponding to each chiral symmetry is an SSH chain with staggered hopping terms.

Given a particular linear path and the respective NN linear chain, the introduction of long-range hopping terms between the odd and even sublattices will not break the chiral symmetry of the linear chain, so one can say each chiral symmetry corresponds to a particular region of the ladder tight-binding parameter space. Furthermore, besides the region where the chiral symmetry is present, there is a region of influence of chiral symmetry which is the region in the hopping parameter space of the general Hamiltonian (that does not have chiral symmetry due to the long-range hoppings) where the Hamiltonian can be adiabatically deformed into the Hamiltonian with chiral symmetry.

In the general case of the ladder, one will have several coexisting choices of linear paths with larger and smaller unit cells as we will see in the next section. If we start from a ladder Hamiltonian with chiral symmetry and the respective shortest unit cell is considered, as one varies the hopping terms, one may approach another chiral symmetry point in the parameter space. If one wants to avoid the existence of hidden symmetries in the respective topological characterization, there are two possibilities: (i) to consider a larger unit cell such that the new chiral operator can be represented in a single unit cell; (ii) to change the indexing of sites in order to obtain the unit cell corresponding to the chiral symmetry point. In the next section, we will illustrate all these arguments in the case of the extended SSH chain.

III. MODEL

In this section, we arrive at the NNN SSH model following a particular reasoning motivated by the indexing problem; that is, we start from the premise that the introduction of long-range hopping should not change the Hamiltonian eigenbasis (it should remain the same as that of the usual SSH chain) in order for the usual chiral operator of the SSH chain to remain a mapping operator between the same eigenstates of the Hamiltonian. This will allow for a comparison between that operator with the new one associated with a new chiral symmetry; see Sec. IV. Note that the extended SSH has been

addressed in the past in several works [10–22], but as far as we know its indexing problem has never been discussed.

Let us then consider a one-dimensional (1D) tight-binding model with nonsymmetric bands $\varepsilon_k^{\pm}$, but with the same eigenbasis of the SSH model, $\{|u_{\pm}(k)\rangle\}$. Note that, since we fixed the eigenbasis, the usual SSH chiral operator $\hat{C}_1|\psi_k^{\pm}\rangle = |k\rangle \otimes \hat{C}_k\,|u_{\pm}(k)\rangle$ is still valid as a mapping operator between eigenstates (a given state in one band has the respective pair in the other band). This chiral operator is written in terms of the Bloch eigenstates $|u_{\pm}(k)\rangle$ of the Hamiltonian H_k as $\hat{C}_1 = \sum_k \hat{C}_1(k)$ with $\hat{C}_1(k) = |u_+(k)\rangle\,\langle u_-(k)| + \text{H.c.}$, with $H_k\,|u_{\pm}(k)\rangle = \varepsilon_{\pm}(k)\,|u_{\pm}(k)\rangle$, and $\varepsilon_+(k) = -\varepsilon_-(k)$ if the bands are symmetric. If the bands are nonsymmetric, one loses the anticommutation relation between this operator and the Hamiltonian (which is no longer bipartite). This implies that the mapping operator is still given by $\hat{C}_1(k) = |u_+(k)\rangle\,\langle u_-(k)| + \text{H.c.}$, but with $\varepsilon_+(k) \neq -\varepsilon_-(k)$. Furthermore, topological invariants such as the Zak's phase that are calculated from this eigenbasis remain exactly the same with quantified values and a discontinuity when $t_1 = t_2$. The matrix representation of $H(k)$ in this eigenbasis is $H(k) = \text{diag}[\varepsilon_+(k), \varepsilon_-(k)]$, where $\varepsilon_+(k) > \varepsilon_-(k)$, $\forall k$, except at a particular choice of the parameters where the gap closes. The matrix representation in the "Wannier" basis $\{|k;A\rangle, |k;B\rangle\}$ is

$$H(k) = \begin{bmatrix} \varepsilon_d(k) & \varepsilon_o(k)e^{-i\phi(k)} \\ \varepsilon_o(k)e^{i\phi(k)} & \varepsilon_d(k) \end{bmatrix}, \tag{1}$$

where we have diagonal terms $\varepsilon_d(k) = [\varepsilon_+(k) + \varepsilon_-(k)]/2$ and off-diagonal terms $\varepsilon_o(k) = [\varepsilon_+(k) - \varepsilon_-(k)]/2$. The above matrix has no σ_z component and that implies that a winding vector can still be defined in the xy plane.

In the case of the usual SSH model, we have $\varepsilon_o(k)e^{i\phi(k)} = t_1 + t_2e^{iak}$ and $\varepsilon_d(k) = 0$, and therefore $\varepsilon_{\pm}(k)e^{i\phi(k)} = \pm(t_1 + t_2e^{iak})$. The Fourier transform of the diagonal terms is zero and the off-diagonal term is $\frac{1}{N}\sum_k e^{ik(j-l)}(t_1 + t_2e^{iak}) = t_1\delta_{jl} + t_2\delta_{j,l+1}$ and $\frac{1}{N}\sum_k e^{ik(j-l)}(t_1 + t_2e^{-iak}) = t_1\delta_{jl} + t_2\delta_{j,l-1}$, so we obtain correctly the SSH model.

In the general case of the Hamiltonian in Eq. (1), we will have long-range hoppings and on-site potentials. In this paper, we consider a simple case where we keep the SSH model conditions except for $\varepsilon_+(k) + \varepsilon_-(k) = 4\alpha\,\cos(ka)$; that is,

$$H(k) = \begin{bmatrix} 2\alpha\,\cos(ka) & t_1 + t_2e^{-iak} \\ t_1 + t_2e^{iak} & 2\alpha\,\cos(ka) \end{bmatrix}. \tag{2}$$

The real-space Hamiltonian in the Wannier basis $\{|j;A\rangle, |l;B\rangle\}$ is obtained from $H_{jl} = \frac{1}{N}\sum_k e^{ik(j-l)}H(k)$. Since $\frac{1}{N}\sum_k e^{ik(j-l)}[\varepsilon_+(k) + \varepsilon_-(k)] = \alpha(\delta_{j,l+1} + \delta_{j,l-1})$ and

$$\begin{aligned} \varepsilon_o(k)e^{i\phi(k)} &= t_1 + t_2e^{iak} \\ &= \sqrt{2t_1t_2\cos(ak) + t_1^2 + t_2^2}\,e^{i\phi(k)}, \end{aligned} \tag{3}$$

one obtains an SSH tight-binding model with next-nearest-neighbor hoppings, as depicted in Fig. 2(a), whose real-space Hamiltonian is written as

$$H = \sum_j [t_1c_{jA}^{\dagger}c_{jB} + t_2c_{jB}^{\dagger}c_{j+1A} \tag{4}$$

$$+ \alpha(c_{jA}^{\dagger}c_{j+1A} + c_{jB}^{\dagger}c_{j+1B}) + \text{H.c.}]. \tag{5}$$

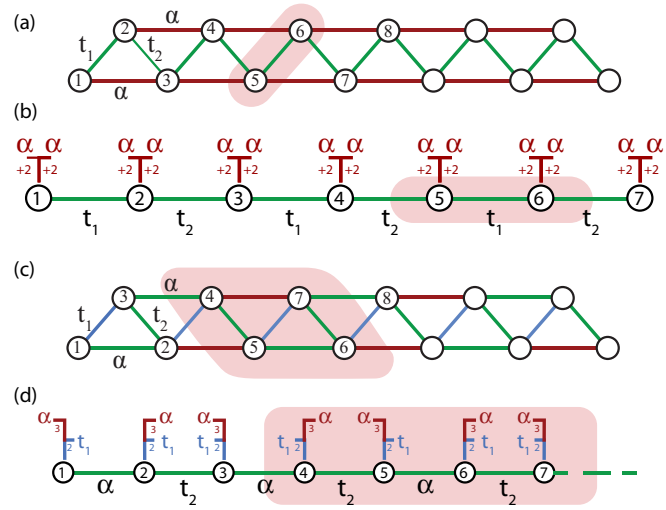

FIG. 2. (a) Usual indexing of the SSH chain with next-nearest-neighbor hopping α. (c) New indexing with the indexing being flipped every other rung. Note that for finite t_1 the unit cell has four sites (and we should consider a ladder with a four-site rung). (b),(d) Linear chain corresponding to the indexing in (a) and (c), respectively, using a shortened representation for the long-range hoppings, whose numbers indicate the distance between connected sites. In (b) [(d)], the red (blue) hopping terms break the bipartite condition (that is, they are hopping terms between sites on the same sublattice).

The respective bands are $\varepsilon_{\pm}(k) = \varepsilon_d(k) \pm |\varepsilon_o(k)|$.

For general values of the hopping parameters, this model falls into the AI symmetry class due to the absence of a chiral symmetry. The chiral symmetry is recovered when the chain becomes bipartite, moving this model into the BDI class [1,2]; that is, it has time reversal, particle-hole, and chiral symmetries.

A. Spectrum of the extended SSH chain

The introduction of NNN hoppings destroys the bipartite property of the SSH chain and this is reflected by the fact that the spectrum is no longer symmetric. In Fig. 3, we show the evolution of the spectrum for the SSH tight-binding model with NNN hopping α for a chain with 21 unit cells plus one site and adopting the indexing of Fig. 2(a). On the right side, $\alpha = 0$ and one has the usual SSH chain with hopping parameters $t_1/t_2 = 2$. This chain has a right edge state (shown on the right of Fig. 3), where the usual subdivision into two sublattices is evident from the fact the edge state has zero amplitudes on one sublattice (indicated by the x symbols), reflecting the usual SSH chiral symmetry. This edge state survives as we increase α, but gains finite amplitude in the latter sublattice. In Fig. 3, we increase α up to 0.2 and then, keeping α fixed, we change t_1 from $t_1/t_2 = 2$ to $t_1/t_2 = 0$ (left limit). The left limiting case again shows a chiral spectrum but with different chiral symmetry reflecting a different unit cell or, equivalently, different choices of sublattices. The need for a different indexing in the left limiting case is signaled by the bottom band inversion at $t_1/t_2 \approx 0.4$ and is evident in the amplitude profile of the corresponding edge state shown on the left (for visual clarity, we show instead the edge state

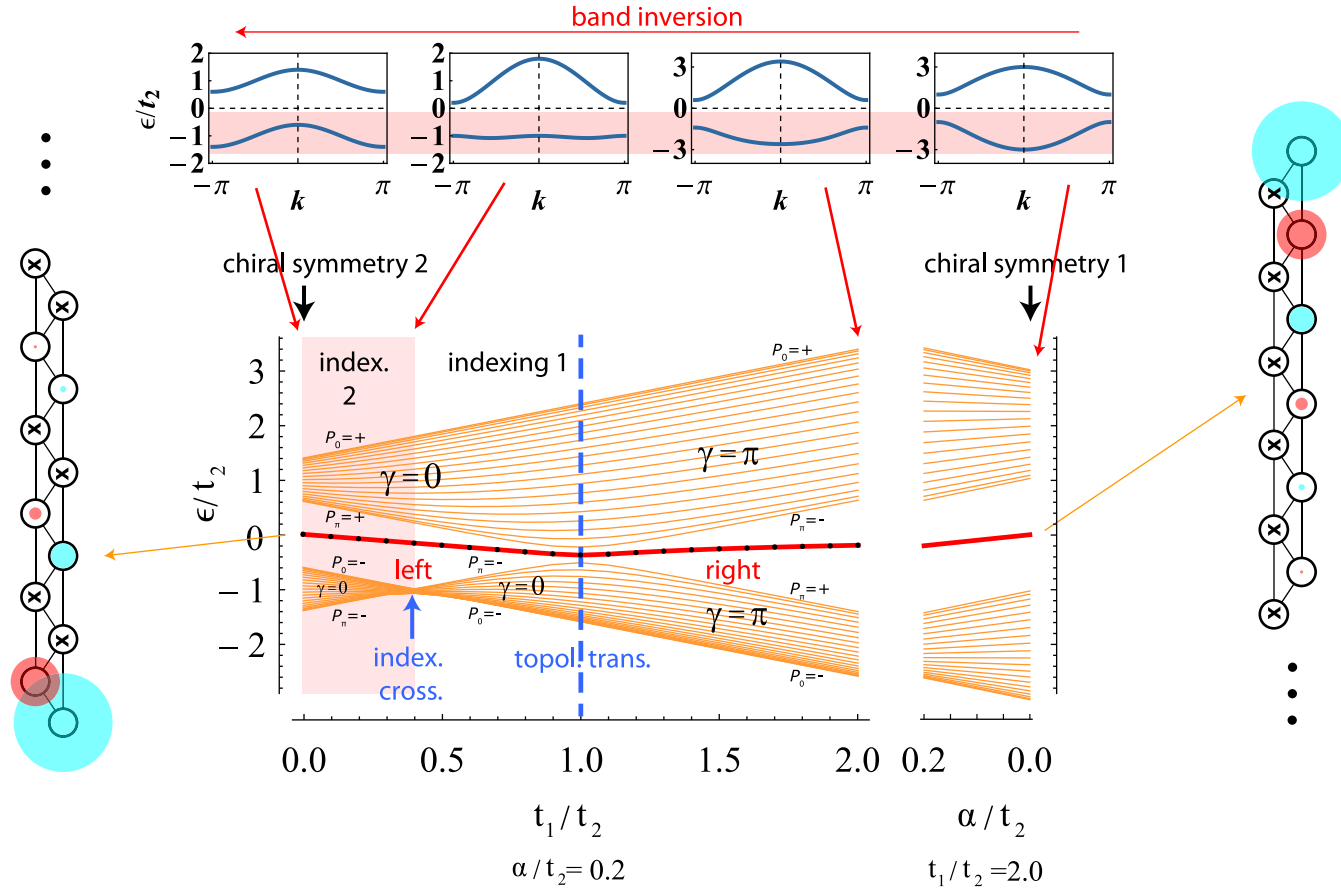

FIG. 3. On the left, spectrum as a function of t_1/t_2 (with $\alpha/t_2 = 0.2$) for the SSH tight-binding model with next-nearest neighbor hopping α for a chain with 21 unit cells plus one site [with a t_1 (t_2) link at the left (right) edge] and adopting the indexing of Fig. 2(a). On the right, spectrum as a function of α/t_2 (with $t_1/t_2 = 2$). The left and right limiting cases show a chiral spectrum, but with different chiral symmetry reflecting a different unit cell or, equivalently, different choices of sublattices. The need for a different indexing in these two cases is signaled by the bottom band inversion and is evident in the amplitude profile of the corresponding edge states shown on the left (for visual clarity, we show instead the edge state corresponding to $\alpha/t_2 = 0.4$) and on the right. The circle sizes indicate the relative amplitudes and the colors reflect the phases (blue is zero; red is π). Parity values and the respective Zak's phases are shown assuming the indexing of Fig. 2(a).

corresponding to $\alpha/t_2 = 0.4$). This band inversion implies multiple level crossings (as shown in Fig. 3) and this implies that the usual reasoning of adiabatic transformation can only be applied from the left (right) to this indexing crossover point. That is, the topological properties to the left of this point ($t_1/t_2 < 0.4$) in Fig. 3 cannot be adiabatically connected to those of the SSH model (with $\alpha = 0$).

Parity values and the respective Zak's phases are also shown in Fig. 3 assuming the indexing of Fig. 2(a). Since the Bloch eigenbasis remains the same throughout this evolution, they are the same as the usual SSH chain, except for the change in parity associated with the bottom band inversion. As in the case of the usual SSH model, a discontinuity in the phases of the components of $|u_1(k)\rangle$ occurs (assuming a smooth gauge) when the gap is closed at $t_1 = t_2$. At this point, the Zak's phase is also discontinuous (and quantified), since it is calculated from the eigenstates of the Hamiltonian (or, equivalently, the parity of the $k = \pi$ states). Another discontinuity is present at the phase of the off-diagonal matrix element of the Block Hamiltonian. Note that, since the eigenstates are the same as that of the usual SSH model, the Hamiltonian has inversion symmetry.

The bottom band inversion is also evident in the left top plot of Fig. 3 as well as the need for a π shift in the bottom band so that the spectrum becomes symmetric as expected due to the presence of a chiral symmetry. It is not possible to describe the latter chiral symmetry using the unit cell of Fig. 2(a), even despite the fact that this remains a perfectly valid unit cell when NNN hoppings are introduced. Therefore, in the general case where $\alpha \neq 0$, other indexings may need to be considered depending on the relative values of the hopping terms. In Fig. 2(c), we show a different possible indexing that implies a four-site unit cell. In Figs. 2(b) and 2(d), the indexings of (a) and (c) are represented in a linear chain where we indicate the long range hoppings using a shortened representation (that may be clearer if one wishes to increase their number).

IV. INDEXING AND CHIRAL SYMMETRY IN LIMITING CASES

To recap, there are two simple limits of our extended SSH model where a chiral symmetry is present.

A. Nearest-neighbor SSH chain ($\alpha = 0$)

Setting $\alpha = 0$ in our extended SSH chain of Fig. 2, there is a natural indexing of sites which is displayed in Fig. 2(a). The maximum number of finite Hamiltonian matrix elements in each row (this is equivalent to the coordination number of each site) is two; then one has a NN tight-binding model and one numbers the sites following the path of finite matrix elements. For this indexing, this bipartite model has a sublattice of even sites connected to the odd sublattice sites in such a way that $t_{ij} \neq 0$ if $|i - j| = 1$. This model has a chiral symmetry and the respective chiral operator is the difference of the projection operators into the even and odd sublattices. This description can be applied to any other limit of the model where a single path of hopping terms is present.

B. Other chiral case $t_1 = 0$

Assuming an even stricter condition, $t_1 = \alpha = 0$, one has decoupled dimers and two flat bands of energies t_2 and $-t_2$ corresponding respectively to bonding and antibonding dimer states. These dimers can be connected in several ways in order to generate chains with only NN hoppings. One is to add horizontal hoppings alternating between the top and the bottom [green lines in Fig. 2(c)] and another is to do it as in the SSH model [green lines in Fig. 2(a)]. This leads to the different indexings in Figs. 2(c) and 2(a). These two ways obviously imply different chiral operators, reflecting the choice of even and odd sublattices.

Considering $t_1 = 0$, $\alpha \neq 0$, and the indexing of Fig. 2(a), the Hamiltonian is $H(k) = 2\alpha \cos(ak)\hat{1} + t_2\hat{\sigma}_x$, where t_2 is assumed as an intracell coupling, and the system can be mapped onto two simple tight-binding chains [of bonding (antibonding) states with on-site potentials t_2 ($-t_2$) and hopping constant α]. These two chains have identical band dispersions apart from the energy shift $2t_2$,

$$\varepsilon_{\pm}(k)/|t_2| = \frac{\alpha}{|t_2|}\cos(ka) \pm 1, \tag{6}$$

with $|u_{\pm}(k)\rangle = [\pm 1 \quad 1]^T/\sqrt{2}$. Apparently this model does not have a chiral symmetry and the absence of a k-dependent phase in $|u_{\pm}(k)\rangle$ may lead one to assume incorrectly that no topological phase can be present. Despite the fact that, at the gap closing point, $t_1 = 0$ and $\alpha/|t_2| = 0.5$, the bands do not touch, a topological transition does occur at this point with the appearance of edge states (note that if one considers a four-site unit cell, this leads to the folding of the bands and the bands touch at the gap closing point). Again, this reflects the fact that the model is bipartite in this limit, but the respective sublattices are not the same as those of the initial SSH model and the respective translational operator of the two-site unit cell is also not the same (see Fig. 2). Therefore, in order to correctly understand the topological phase, the new indexing of the sites of Fig. 2(c) is required.

Let us denote the indexing of Fig. 2(a) by n and the indexing of the sites of Fig. 2(c) by $\bar{n}$. Considering the four-site unit cell of Fig. 2(c) [note that, for $t_1 = 0$, one has a two-site unit cell with the indexing of Fig. 2(c) as easily concluded from Fig. 2(d), but the four-site unit cell makes the change of indexing easier to understand], then the bonding (+) and antibonding (−) states are

$$|\psi_n(k)\rangle_{\pm} = |2k\rangle \otimes \begin{bmatrix}\psi_4\\ \psi_5\\ \psi_6\\ \psi_7\end{bmatrix}_{\pm} = \frac{1}{2}|2k\rangle \otimes \begin{bmatrix}\pm 1\\ 1\\ \pm e^{ika}\\ e^{ika}\end{bmatrix}, \tag{7}$$

and using the new indexing they become

$$|\psi_{\bar{n}}(k)\rangle_{\pm} = |2k\rangle \otimes \begin{bmatrix}\psi_{\bar{4}}\\ \psi_{\bar{5}}\\ \psi_{\bar{6}}\\ \psi_{\bar{7}}\end{bmatrix}_{\pm} = |2k\rangle \otimes \begin{bmatrix}\psi_4\\ \psi_5\\ \psi_7\\ \psi_6\end{bmatrix}_{\pm}$$
$$= \frac{1}{2}|2k\rangle \otimes \begin{bmatrix}\pm 1\\ 1\\ e^{ika}\\ \pm e^{ika}\end{bmatrix}. \tag{8}$$

Therefore, the band of bonding states is the same for both indexings, but in the case of the antibonding band the Bloch eigenstates, when using the indexing of Fig. 2(c) and a two-site unit cell, become $|k + \pi\rangle \otimes |u_-(k + \pi)\rangle$ and this implies a π shift in the momentum of the bottom band.

The bulk Hamiltonian of the chain in Fig. 2(d), assuming a unit cell of sites $\{2, 3\}$ and $t_1 = 0$, is $H(k) = [t_2 + 2\alpha \cos(ak)]\hat{\sigma}_x$, the eigenvalues are $\pm[t_2 + 2\alpha \cos(ak)]$, and the respective eigenstates are again $|u_{\pm}(k)\rangle = [\pm 1 \quad 1]^T/\sqrt{2}$, that is, they are independent of k for this choice of unit cell. The respective Zak's phase is zero for both bands and this is expected since, if the site 1 is absent in Fig. 2(d), no edge state will be present. The same occurs in the case of the old indexing of Fig. 2(b), but note that a shift of one site in the unit cell leads to a finite Zak's phase and this agrees with the fact that for the choice of OBC of Fig. 2 an edge state is observed.

The correct chiral operator $\mathcal{C}_2$ that protects the edge states in this case requires two two-site unit cells if one works with the indexing of sites in Fig. 2(a), but a single two-site unit cell using the indexing of sites in Fig. 2(c). Using the former indexing, we have in the Wannier basis of two unit cells

$$\mathcal{C}_2 = \begin{bmatrix}1 & 0 & 0 & 0\\ 0 & -1 & 0 & 0\\ 0 & 0 & -1 & 0\\ 0 & 0 & 0 & 1\end{bmatrix}, \tag{9}$$

or in the two-band Bloch basis,

$$\mathcal{C}_2(k) = |\varepsilon_{k,+}\rangle\langle\varepsilon_{k+\pi,-}| + |\varepsilon_{k,-}\rangle\langle\varepsilon_{k+\pi,+}| + \text{H.c.}, \tag{10}$$

or, equivalently,

$$\mathcal{C}_2 H(k)\mathcal{C}_2^{-1} = -H(k + \pi). \tag{11}$$

Similar operators have been found in Refs. [5,6]. This expression implies that by using the indexing of Fig. 2(a) the chiral operator $\mathcal{C}_2$ cannot be defined as an operator acting only in $|u_{\pm}(k)\rangle$ as in the case of the SSH model (unless we use a larger unit cell with four sites) and, in fact, this operator reflects a hidden chiral symmetry for that indexing. If the indexing of Fig. 2(c) is used, the chiral operator $\mathcal{C}_2$ can now be written as an operator (with the usual form) acting only in $|u_{\pm}(k)\rangle$, but not the chiral operator $\mathcal{C}_1$, that is, the chiral symmetry of the SSH chain becomes a hidden chiral symmetry if we choose the indexing of Fig. 2(c). Note that this implies that, since the

edge states for $t_1 = 0$ are eigenstates of this chiral operator $\mathcal{C}_2$, the "unit cell" for the edge state shown at the left of Fig. 3 has four sites using the indexing of Fig. 2(a) and two sites using the indexing of Fig. 2(c).

V. EDGE STATES OF THE EXTENDED SSH CHAIN

Let us now discuss the characteristics of the edge states in the general case where $t_1 \neq 0$ and $\alpha \neq 0$. In several recent works [23–29], it has been assumed that edge states in 1D topological insulators can be determined from the bulk Hamiltonian using the substitution $e^{ik} \to c$ in the bulk Hamiltonian, reflecting the assumption of an ansatz

$$|\psi_{edge}\rangle_j = c^j |u(c)\rangle = c^j \begin{bmatrix} \psi_A \\ \psi_B \end{bmatrix} \tag{12}$$

(where j is the unit cell index) in the eigenvalue equation of the infinite system. Here we show that the presence of long-range hopping in the SSH chain modifies this ansatz, due to the competition of the two chiral symmetries associated with the two limits $t_1 = 0$ and $\alpha = 0$ (reflecting the two indexings of Fig. 2 and the respective even and odd sublattices).

Assuming the unit cell ($A = 5, B = 6$) shown in Fig. 2(a), the eigenvalue equation for the edgelike states in the infinite chain generates the following equations:

$$\varepsilon c^j \psi_A = \alpha \psi_A c^{j-1} + \alpha \psi_A c^{j+1} + t_1 \psi_B c^j + t_2 \psi_B c^{j-1}, \tag{13}$$

$$\varepsilon c^j \psi_B = t_1 \psi_A c^j + t_2 \psi_A c^{j+1} + \alpha \psi_B c^{j-1} + \alpha \psi_B c^{j+1}, \tag{14}$$

which can be rewritten as a matrix equation:

$$\varepsilon \begin{bmatrix} \psi_A \\ \psi_B \end{bmatrix} = \begin{bmatrix} \alpha(c + 1/c) & t_1 + t_2/c \\ t_1 + t_2 c & \alpha(c + 1/c) \end{bmatrix} \begin{bmatrix} \psi_A \\ \psi_B \end{bmatrix}. \tag{15}$$

The respective characteristic polynomial is *quadratic* in c (and quadratic in ε) if $\alpha = 0$, but becomes *quartic* in c (remaining quadratic in ε) if $\alpha \neq 0$. Therefore, for each energy value ε, we have two c solutions [one corresponding to a left edge state and the other to a right edge state; see Fig. 4(a)] if $\alpha = 0$, but four solutions if $\alpha \neq 0$ [see Fig. 4(b)]. The latter implies in certain energy intervals the existence of two right (left) edge eigenstates in the infinite chain [states with decay in the right (left) direction] that may be combined in order to generate a single right (left) edge state with zero amplitudes at all the sites of a unit cell of the chain, so that OBC may be introduced at these sites [12]. Note that, while in the case of the SSH model with OBC, a single condition selects the left edge state from the set of left edgelike states of the infinite chain and that condition is that of zero amplitude at a virtual site at the left end (that will also impose zero amplitude in the respective sublattice), when we have two left edge states in the infinite chain with the same energy we need two conditions (these will be the zeros of amplitude at the two virtual sites A and B to the left of the chain so that the resulting eigenstate of the infinite chain does not "feel" the OBC).

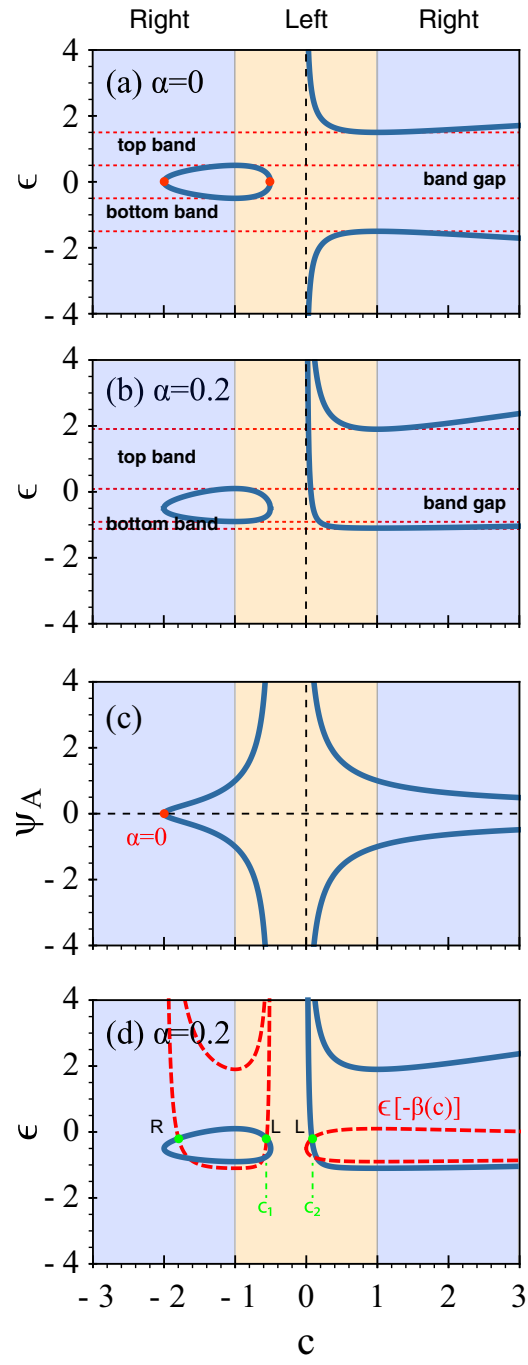

FIG. 4. (a), (b) Real c roots (corresponding to edgelike states of the infinite chain) of the characteristic polynomial of the c matrix in Eq. (15) and the respective energy for $t_1 = 0.5$, $t_2 = 1$, (a) $\alpha = 0$, or (b) $\alpha = 0.2$. In the case of $\alpha = 0$, there two possible values of c for each energy in the band gap (corresponding to a right and a left edgelike state). When NNN hopping is present ($\alpha = 0.2$), four c values are present in the band gap region, with one of the right edge solutions outside the range of this plot. (c) Amplitude ψ_A of the eigenstate in Eq. (18) as a function of real c. (d) The intersection of the curves $\varepsilon_\pm(c)$ and $\varepsilon_\pm[-\gamma(c)]$ gives us the c_1 and c_2 values present in the edge state [with amplitudes of the form $\psi_{A/B}(c_1^j - c_2^j)$].

The eigenvalues ε as functions of c are

$$\varepsilon_\pm(c) = \frac{\alpha c^2 + \alpha \pm \beta}{c}, \quad \beta = \sqrt{c(ct_1 + t_2)(t_1 + ct_2)} \tag{16}$$

and the respective eigenstates are

$$c^j\begin{bmatrix}\psi_A\\ \psi_B\end{bmatrix} = c^j\begin{bmatrix}1\\ \pm\dfrac{\beta}{ct_1+t_2}\end{bmatrix} = c^j\begin{bmatrix}1\\ \pm\sqrt{c\gamma(c)}\end{bmatrix}, \tag{17}$$

or equivalently

$$c^j\begin{bmatrix}\psi_A\\ \psi_B\end{bmatrix} = c^j\begin{bmatrix}\pm\dfrac{ct_1+t_2}{\beta}\\ 1\end{bmatrix} = c^j\begin{bmatrix}\pm\dfrac{1}{\sqrt{c\gamma(c)}}\\ 1\end{bmatrix}, \tag{18}$$

where

$$\gamma(c) = \frac{t_1+ct_2}{ct_1+t_2} \tag{19}$$

and where we have assumed that $ct_1 + t_2$ is positive in the last equality of Eqs. (18) and (17). Note that the amplitudes do not depend on α.

For $\alpha = 0$, the edge state energy is determined imposing $\psi_A = 0$ in Eq. (18) or $\psi_B = 0$ in Eq. (17). This implies $c = -t_2/t_1$ or $c = -t_1/t_2$, and, depending on the value of the ratio t_1/t_2, these will be left or right edge states. In both situations, the respective energy given by Eq. (16) will be zero. These energies and the amplitude are indicated in Figs. 4(a) and 4(c), respectively, by the red dots.

For $\alpha \neq 0$, if the edge state has two consecutive zeros of amplitude (this implies a unit cell with zero amplitudes) in the chain, OBC may be introduced at the B site (the left edge) and one obtains an eigenstate of the semi-infinite chain which is orthogonal to the bulk eigenstates. Let us determine the energy of such an edge state. As explained above, the existence of this edge state requires for finite α the presence of four real c solutions of the characteristic equation, two of them corresponding to left edgelike states; see Fig. 4(b) (one of the right edge solutions is outside the range of this plot). The left edge state is obtained combining two left edgelike states with the same energy that can be written as

$$|L_1\rangle_j = c_1^j\begin{bmatrix}1\\ \psi_B(c_1)\end{bmatrix}, \tag{20}$$

$$|L_2\rangle_j = c_2^j\begin{bmatrix}1\\ \psi_B(c_2)\end{bmatrix}. \tag{21}$$

Since we have NNN hoppings, in order for a linear combination of these two states to be an eigenstate of the chain with OBC (or better, of a semi-infinite chain), the amplitudes at both virtual sites (the unit cell with $j = 0$) must be zero,

$$a\begin{bmatrix}1\\ \psi_B(c_1)\end{bmatrix} + b\begin{bmatrix}1\\ \psi_B(c_2)\end{bmatrix} = \begin{bmatrix}0\\ 0\end{bmatrix} \Rightarrow \begin{cases}a=-b,\\ \psi_B(c_1)=\psi_B(c_2),\end{cases} \tag{22}$$

that is, $|edge\rangle = |L_1\rangle - |L_2\rangle$ and the energy of the edge state is determined by the condition that at that energy one has two left (or two right) edgelike eigenstates of the infinite chain that have the same unit cell amplitudes (apart from the decaying factor). The relation between c_1 and c_2 is simple,

$$\psi_B(c_1) = \psi_B(c_2) \Rightarrow c_1\gamma(c_1) = c_2\gamma(c_2) \Rightarrow \begin{cases}c_1 = -\gamma(c_2),\\ c_2 = -\gamma(c_1).\end{cases} \tag{23}$$

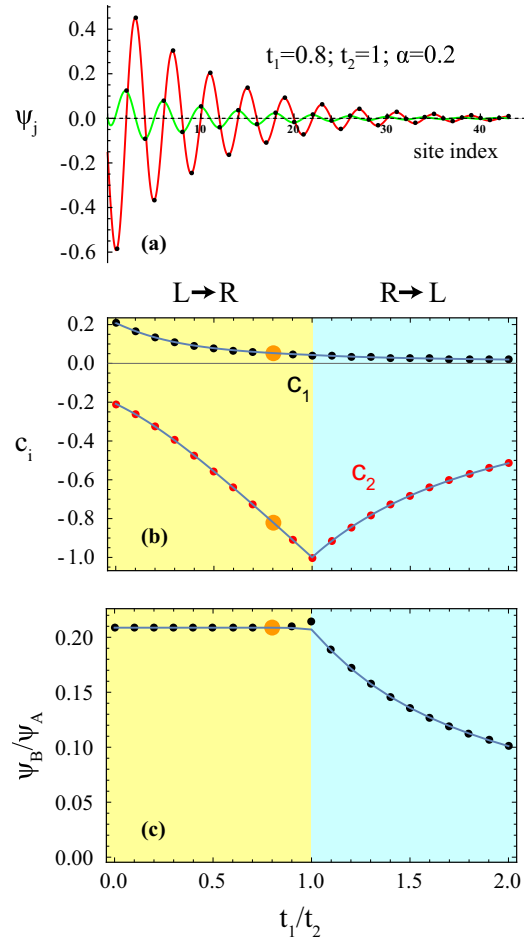

FIG. 5. (a) Edge state amplitudes for $t_1 = 0.8$, $t_2 = 1$, and $\alpha = 0.2$ assuming the indexing of Fig. 2(a). The red and green curves are fits of the form $\psi_{A/B}(c_1^j - c_2^j)$ for respectively the A and B sublattices. (b) c_1 and c_2 values and (c) ψ_B/ψ_A extracted from the fits. The dots in (b) and (c) are numerical data extracted from fits to the edge state amplitudes as shown in (a) and the lines are plotted from the theoretical results [Eq. (25) with $X(x)$ given by Eq. (28) in the case of the c values shown in (b) and Eq. (17) in the case of the amplitudes ratio shown in (c)]. For $t_1/t_2 > 1$, one has a right edge state for chain endings as in Fig. 2(a) and, in order to keep the c values continuous, the indexing is flipped, that is, we index the sites from the right to the left. The edge state in (a) corresponds to the orange dots in (b) and (c).

The last two relations are equivalent. This edge state can be written as

$$|edge\rangle_j = \{c^j - [-\gamma(c)]^j\}\begin{bmatrix}1\\ \psi_B(c)\end{bmatrix}. \tag{24}$$

One can also conclude from Fig. 4(d) that c_1 and c_2 have opposite signs.

In Fig. 5(a), we show an example of amplitude profile of an edge state (for $t_1 = 0.8$, $t_2 = 1$, and $\alpha = 0.2$) assuming the indexing of Fig. 2(a). The red and green curves are fits of the form $\psi_{A/B}(c_1^j - c_2^j)$ for respectively the A and B sublattices. We considered just the largest amplitude points for the fits since finite size effects should introduce deviations in the tail of the edge state (due to the presence of the other boundary).

In Fig. 5(b), we show the c_1 and c_2 values and in Fig. 5(c) ψ_B/ψ_A as t_1/t_2 grows for fixed $\alpha = 0.2$. The dots in Figs. 5(b) and 5(c) are numerical data extracted from fits to the edge state amplitudes as shown in Fig. 5(a) (the red and green fits generate the same values of c_1 and c_2) and the lines are plotted from the theoretical results—Eq. (25) with $X(x)$ given by Eq. (28) in the case of the c values and Eq. (17) in the case of the amplitudes ratio, as we explain below. An almost perfect fit is found with a small deviation at the topological transition point. For $t_1/t_2 > 1$, one has a right edge state for chain endings as in Fig. 2(a) and, in order to keep the c values continuous, the indexing is flipped, that is, we index the sites from the right to the left. The edge state in Fig. 5(a) corresponds to the orange dots in Figs. 5(b) and 5(c).

Note that Fig. 5(c) shows that $\psi_B(c)$ (setting $\psi_A = 1$) is a function of only α/t_2 for $t_1 < t_2$, $\psi_B(c) = \pm X(\alpha/t_2)$. The apparent lack of symmetry for $t_1 > t_2$ just reflects the fact that, in this region, $\psi_B(c)$ (setting $\psi_A = 1$) is a function of α/t_1 (due to the symmetry $t_1 \leftrightarrow t_2 \ \oplus \ \mathrm{L} \leftrightarrow \mathrm{R}$), $\psi_B(c) = \pm\sqrt{c/\gamma(c)} = \pm X(\alpha/t_1)$, and therefore $\psi_B(c)$ changes as t_1 grows for fixed α. So we have

$$\psi_B(c) = \pm\begin{cases}\sqrt{c\gamma(c)}, & \text{for } t_1 < t_2,\\ \sqrt{c/\gamma(c)}, & \text{for } t_1 > t_2,\end{cases}$$
$$= \pm\begin{cases}X(\alpha/t_2), & \text{for } t_1 < t_2,\\ X(\alpha/t_1), & \text{for } t_1 > t_2.\end{cases} \tag{25}$$

This equation determines the value of c if the function $X(x)$ is known.

The function $X(x)$ [and the value of c in Eq. (24)] is determined by the condition that the left edge states $|L_1\rangle_j$ and $|L_2\rangle_j$ have the same energy, $\varepsilon_\pm(c_1) = \varepsilon_\pm(c_2)$ (and the same reasoning applies to right edge states), and this leads to

$$\varepsilon_\pm(c) = \varepsilon_\pm[-\gamma(c)]. \tag{26}$$

That is, the intersection of the curves $\varepsilon_\pm(c)$ and $\varepsilon_\pm[-\gamma(c)]$ gives us the exact form of the edge state [see Fig. 4(d)]. For $t_1/t_2 = 1/2$, one has $\varepsilon_\pm(c) = \alpha/t_2$.

Since $X(\alpha/t_2)$ is independent of t_1 for $t_1 < t_2$, we may determine this function in the simple case $t_1 = 0$. For $t_1 = 0$, one has $\gamma(c) = c$, $\psi_B = \pm c$, $\beta = |ct_2|$ and $\varepsilon_\pm(c) = \varepsilon_\pm(-c)$ leads to

$$c = X(\alpha/t_2), \tag{27}$$

with

$$X(x) = \frac{\pm 1 \pm \sqrt{1 - 4x^2}}{2x}, \tag{28}$$

where the four combinations must be considered (generating two left and two right edge states). So, to conclude, with the above expression for $X(x)$, Eq. (25) determines the value of c_1 [c_2 being $-\gamma(c_1)$] and Eq. (16) gives the respective edge state energy.

To complete our analysis of the effect of long range hopping on the topological edge states, we show in Fig. 6 log plots of the absolute values of the edge state amplitudes as a function of site index using the usual indexing, for several values of t_1 and α ($t_2 = 1$). The log plot in Fig. 6(a), with $\alpha \ll t_1$, reflects the existence of the two sublattices associated with the indexing of Fig. 2(a) (due to the proximity to the SSH chiral symmetry point), while the log plot in Fig. 6(f) displays a doubling of the edge state unit cell, reflecting the need for a different indexing with a new unit cell that generates the sublattices shown in Fig. 6(f). The change from the $\mathcal{C}_1$ SSH chiral symmetry [reflected by the separation into two sublattices in (a)] to the $\mathcal{C}_2$ chiral symmetry [corresponding to two different sublattices in (f)] is gradual, occurring first at the edge of the edge state [see red arrows in (c) and (d)]. If we replot these data using the new indexing of Fig. 2(c), the behavior for small and large t_1/α is exchanged.

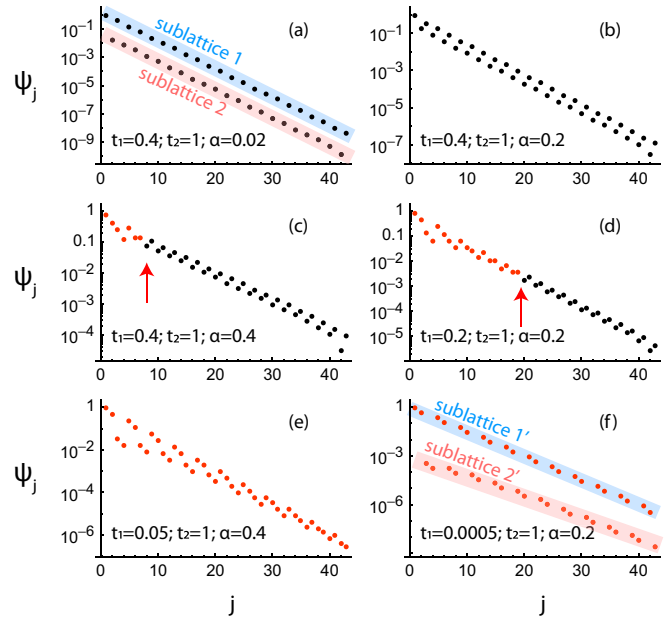

FIG. 6. Log plot of the absolute values of the edge state amplitudes as a function of site index using the usual indexing, for several values of t_1 and α ($t_2 = 1$). The change from the t_1-t_2 SSH chiral symmetry [reflected by the separation into two sublattices in (a)] to the other [corresponding to two different sublattices in (f)] is gradual, occurring first at the edge of the edge state [see red arrows in (c) and (d)]. As t_1 approaches zero, $c_2 \to -c_1$ and a doubling of the edge state "unit cell" is observed, reflecting the need for a different indexing. If we replot these data using the new indexing of Fig. 2(c), the behavior for small and large t_1/α is exchanged. In (a)–(f), the edge state amplitudes that show the doubling of the edge state unit cell (and reflect the existence of the sublattices $1'$ and $2'$) are colored in red. The edge state amplitudes given by the black dots reflect the usual bipartition of the SSH chain.

VI. CONCLUSION

The characterization of topological insulators depends strongly on its set of symmetries. In the case of translational invariant Hamiltonians, these symmetries can be written as a set of well known equations that involve the bulk Hamiltonian and the respective symmetry operator. The bulk Hamiltonian reflects a choice of unit cell and it is usually assumed that any choice of unit cell will allow one to fully characterize a topological insulator. In this paper, we argue that this is not always correct and that several choices of unit cell or, equivalently, of site indexing should be considered in the case of linear chains with long range hoppings in order to describe

their bulk topological behavior. Otherwise, depending on the relative values of the hopping parameters, hidden symmetries may be present [5–9]. We have exemplified the above arguments considering the particular case of the extended SSH chain. In this model, the introduction of long-range hopping terms breaks in general the bipartite property causing the Hamiltonian to lose its respective chiral symmetry, and a band inversion occurs in the band structure as the relative values of the hopping terms change. We have shown this band inversion signals a crossover between hopping parameter regions of "influence" of different chiral symmetries and that, depending on the choice of unit cell, these may be hidden chiral symmetries.

We have also shown that, as a consequence of the long-range terms, the edge states of the extended SSH chain become a linear combination of two edgelike states with different localization lengths but equal amplitudes in the unit cell (apart from the decaying term). We have determined the exact form of these edge states and of the respective energy for any value of the next-nearest hopping term. When one of the nearest-neighbor hopping parameters becomes small compared with the next-nearest-neighbor hopping parameter, the localization lengths become similar and this implies the gradual appearance of a chiral symmetry different from that of the SSH (edge states being protected by this new chiral symmetry when a nearest-neighbor hopping parameter is zero) that reflects a new sublattice distribution of the lattice sites and the need for a new indexing of the lattice sites. This need is also signaled by the inversion of one of the model bands.

Similar behavior to that of the extended SSH chain should be present in other bipartite 1D [27,30–32] and 2D [33–36] topological insulators if long-range hopping terms are introduced. A simple 2D example where the approach of this paper can be applied is that of a plane of parallel extended SSH chains with uniform or staggered hopping terms between them. An interesting extension of these results should also be possible in the context of square-root topological insulators [30,31,37] or the recently proposed 2^n-root topological insulators [38–40]. We also expect the introduction of long-range hopping terms in higher-order topological insulators [41–43] to raise similar concerns about the possibility of hidden symmetries as well as the existence of multiple localization lengths in the corner states. An open question is the effect of disorder in what concerns the linear combination of edgelike states with different localization lengths.

The experimental observation of the features described in this paper should be realizable in artificial lattices such as ultracold atoms in optical lattices [44], photonic crystals [45], topolectrical circuits [46–49], acoustic lattices [50,51], vacancy lattices [52], or atoms or molecules on surfaces [53]. Since the hopping terms are decreasing functions of the distance between sites (except in topolectrical circuits) the extended SSH realization should adopt the geometry of Fig. 2(a), but for example with a scalene t_1-t_2-α triangle where the largest side corresponds to the smallest hopping parameter $t_{1,2}$.

ACKNOWLEDGMENTS

This work was developed within the scope of the Portuguese Institute for Nanostructures, Nanomodelling and Nanofabrication (i3N) Projects No. UIDB/50025/2020 and No. UIDP/50025/2020. R.G.D. and A.M.M. acknowledge funding from FCT–Portuguese Foundation for Science and Technology through Project No. PTDC/FIS-MAC/29291/2017. A.M.M. acknowledges financial support from the FCT through the work Contract No. CDL-CTTRI-147-ARH/2018.

[1] A. Altland and M. R. Zirnbauer, Nonstandard symmetry classes in mesoscopic normal-superconducting hybrid structures, Phys. Rev. B **55**, 1142 (1997).

[2] C.-K. Chiu, J. C. Y. Teo, A. P. Schnyder, and S. Ryu, Classification of topological quantum matter with symmetries, Rev. Mod. Phys. **88**, 035005 (2016).

[3] J. Zak, Berry's Phase for Energy Bands in Solids, Phys. Rev. Lett. **62**, 2747 (1989).

[4] J. K. Asbóth, L. Oroszlány, and A. Pályi, *A Short Course on Topological Insulators*, Lecture Notes in Physics Vol. 919 (Springer, Berlin, 2016).

[5] L. Li and S. Chen, Hidden-symmetry–protected topological phases on a one-dimensional lattice, EPL (Europhys. Lett.) **109**, 40006 (2015).

[6] J. Zurita, C. Creffield, and G. Platero, Tunable zero modes and quantum interferences in flat-band topological insulators, Quantum **5**, 591 (2021).

[7] T. Fukui, K.-I. Imura, and Y. Hatsugai, Symmetry protected weak topological phases in a superlattice, J. Phys. Soc. Jpn. **82**, 073708 (2013).

[8] J.-M. Hou and W. Chen, Hidden-symmetry-protected quantum pseudo–spin Hall effect in optical lattices, Phys. Rev. A **93**, 063626 (2016).

[9] J.-M. Hou and W. Chen, Hidden symmetry-protected Z_2 topological insulator in a cubic lattice, Phys. Rev. B **96**, 235108 (2017).

[10] H.-C. Hsu and T.-W. Chen, Topological Anderson insulating phases in the long-range Su-Schrieffer-Heeger model, Phys. Rev. B **102**, 205425 (2020).

[11] M. Maffei, A. Dauphin, F. Cardano, M. Lewenstein, and P. Massignan, Topological characterization of chiral models through their long time dynamics, New J. Phys. **20**, 013023 (2018).

[12] B.-H. Chen and D.-W. Chiou, An elementary rigorous proof of bulk-boundary correspondence in the generalized Su-Schrieffer-Heeger model, Phys. Lett. A **384**, 126168 (2020).

[13] N. Ahmadi, J. Abouie, and D. Baeriswyl, Topological and nontopological features of generalized Su-Schrieffer-Heeger models, Phys. Rev. B **101**, 195117 (2020).

[14] S.-L. Zhang and Q. Zhou, Two-leg Su-Schrieffer-Heeger chain with glide reflection symmetry, Phys. Rev. A **95**, 061601(R) (2017).

[15] S. Rolston, Extended SSH model: Non-local couplings and non-monotonous edge states, Physics **1**, 2 (2008).

[16] D. Xie, W. Gou, T. Xiao, B. Gadway, and B. Yan, Topological characterizations of an extended Su-Schrieffer-Heeger model, npj Quantum Inf. **5**, 55 (2019).

[17] Z. Fu, N. Fu, H. Zhang, Z. Wang, D. Zhao, and S. Ke, Extended SSH model in non-Hermitian waveguides with alternating real and imaginary couplings, Appl. Sci. **10**, 3425 (2020).

[18] B. Pérez-González, M. Bello, A. Gómez-León, and G. Platero, Interplay between long-range hopping and disorder in topological systems, Phys. Rev. B **99**, 035146 (2019).

[19] B. Pérez-González, M. Bello, Á. Gómez-León, and G. Platero, SSH model with long-range hoppings: topology, driving and disorder, arXiv:1802.03973 [cond-mat.mes-hall].

[20] S. Longhi, Probing one-dimensional topological phases in waveguide lattices with broken chiral symmetry, Opt. Lett. **43**, 4639 (2018).

[21] B. Hetényi, Y. Pulcu, and S. Doğan, Calculating the polarization in bipartite lattice models: Application to an extended Su-Schrieffer-Heeger model, Phys. Rev. B **103**, 075117 (2021).

[22] L. Li, Z. Xu, and S. Chen, Topological phases of generalized Su-Schrieffer-Heeger models, Phys. Rev. B **89**, 085111 (2014).

[23] P. Delplace, D. Ullmo, and G. Montambaux, Zak phase and the existence of edge states in graphene, Phys. Rev. B **84**, 195452 (2011).

[24] L. Banchi and R. Vaia, Spectral problem for quasi-uniform nearest-neighbor chains, J. Math. Phys. **54**, 043501 (2013).

[25] D. Hügel and B. Paredes, Chiral ladders and the edges of quantum Hall insulators, Phys. Rev. A **89**, 023619 (2014).

[26] C. W. Duncan, P. Öhberg, and M. Valiente, Exact edge, bulk, and bound states of finite topological systems, Phys. Rev. B **97**, 195439 (2018).

[27] A. M. Marques and R. G. Dias, One-dimensional topological insulators with noncentered inversion symmetry axis, Phys. Rev. B **100**, 041104(R) (2019).

[28] A. M. Marques and R. G. Dias, Analytical solution of open crystalline linear 1d tight-binding models, J. Phys. A: Math. Theor. **53**, 075303 (2020).

[29] T. Fukui, Theory of edge states based on the Hermiticity of tight-binding Hamiltonian operators, Phys. Rev. Res. **2**, 043136 (2020).

[30] M. Kremer, I. Petrides, E. Meyer, M. Heinrich, O. Zilberberg, and A. Szameit, A square-root topological insulator with non-quantized indices realized with photonic Aharonov-Bohm cages, Nat. Commun. **11**, 907 (2020).

[31] G. Pelegrí, A. M. Marques, R. G. Dias, A. J. Daley, V. Ahufinger, and J. Mompart, Topological edge states with ultracold atoms carrying orbital angular momentum in a diamond chain, Phys. Rev. A **99**, 023612 (2019).

[32] G. Pelegrí, A. M. Marques, R. G. Dias, A. J. Daley, J. Mompart, and V. Ahufinger, Topological edge states and Aharanov-Bohm caging with ultracold atoms carrying orbital angular momentum, Phys. Rev. A **99**, 023613 (2019).

[33] T. Du, Y. Li, H. Lu, and H. Zhang, Effects of correlations on phase diagrams of the two-dimensional Su–Schrieffer–Heeger model with the larger topological invariant, Physica E **134**, 114884 (2021).

[34] F. Liu and K. Wakabayashi, Novel Topological Phase with a Zero Berry Curvature, Phys. Rev. Lett. **118**, 076803 (2017).

[35] D. Obana, F. Liu, and K. Wakabayashi, Topological edge states in the Su-Schrieffer-Heeger model, Phys. Rev. B **100**, 075437 (2019).

[36] L. Madail, S. Flannigan, A. M. Marques, A. J. Daley, and R. G. Dias, Enhanced localization and protection of topological edge states due to geometric frustration, Phys. Rev. B **100**, 125123 (2019).

[37] J. Arkinstall, M. H. Teimourpour, L. Feng, R. El-Ganainy, and H. Schomerus, Topological tight-binding models from nontrivial square roots, Phys. Rev. B **95**, 165109 (2017).

[38] A. M. Marques, L. Madail, and R. G. Dias, One-dimensional 2^n-root topological insulators and superconductors, Phys. Rev. B **103**, 235425 (2021).

[39] R. G. Dias and A. M. Marques, Matryoshka approach to sine-cosine topological models, Phys. Rev. B **103**, 245112 (2021).

[40] A. M. Marques and R. G. Dias, 2^n-root weak, Chern and higher-order topological insulators and 2^n-root topological semimetals, Phys. Rev. B **104**, 165410 (2021).

[41] W. A. Benalcazar, B. A. Bernevig, and T. L. Hughes, Electric multipole moments, topological multipole moment pumping, and chiral hinge states in crystalline insulators, Phys. Rev. B **96**, 245115 (2017).

[42] F. Schindler, A. M. Cook, M. G. Vergniory, Z. Wang, S. S. P. Parkin, B. A. Bernevig, and T. Neupert, Higher-order topological insulators, Sci. Adv. **4**, eaat0346 (2018).

[43] G. Pelegrí, A. M. Marques, V. Ahufinger, J. Mompart, and R. G. Dias, Second-order topological corner states with ultracold atoms carrying orbital angular momentum in optical lattices, Phys. Rev. B **100**, 205109 (2019).

[44] M. Leder, C. Grossert, L. Sitta, M. Genske, A. Rosch, and M. Weitz, Real-space imaging of a topologically protected edge state with ultracold atoms in an amplitude-chirped optical lattice, Nat. Commun. **7**, 13112 (2016).

[45] N. Parappurath, F. Alpeggiani, L. Kuipers, and E. Verhagen, Direct observation of topological edge states in silicon photonic crystals: Spin, dispersion, and chiral routing, Sci. Adv. **6**, eaaw4137 (2020).

[46] S. Imhof *et al.*, Topolectrical-circuit realization of topological corner modes, Nat. Phys. **14**, 925 (2018).

[47] S. Liu, W. Gao, Q. Zhang, S. Ma, L. Zhang, C. Liu, Y. J. Xiang, T. J. Cui, and S. Zhang, Topologically protected edge state in two-dimensional Su-Schrieffer-Heeger circuit, Research **2019**, 8609875 (2019).

[48] N. A. Olekhno, E. I. Kretov, A. A. Stepanenko, P. A. Ivanova, V. V. Yaroshenko, E. M. Puhtina, D. S. Filonov, B. Cappello, L. Matekovits, and M. A. Gorlach, Topological edge states of interacting photon pairs emulated in a topolectrical circuit, Nat. Commun. **11**, 1436 (2020).

[49] C. H. Lee, S. Imhof, C. Berger, F. Bayer, J. Brehm, L. W. Molenkamp, T. Kiessling, and R. Thomale, Topolectrical circuits, Commun. Phys. **1**, 39 (2018).

[50] B. G.-g. Chen, N. Upadhyaya, and V. Vitelli, Nonlinear conduction via solitons in a topological mechanical insulator, Proc. Natl. Acad. Sci. USA **111**, 13004 (2014).

[51] L.-Y. Zheng, V. Achilleos, O. Richoux, G. Theocharis, and V.

Pagneux, Observation of Edge Waves in a Two-Dimensional Su-Schrieffer-Heeger Acoustic Network, Phys. Rev. Appl. **12**, 034014 (2019).

[52] R. Drost, T. Ojanen, A. Harju, and P. Liljeroth, Topological states in engineered atomic lattices, Nat. Phys. **13**, 668 (2017).

[53] M. R. Slot, T. S. Gardenier, P. H. Jacobse, G. C. P. van Miert, S. N. Kempkes, S. J. M. Zevenhuizen, C. M. Smith, D. Vanmaekelbergh, and I. Swart, Experimental realization and characterization of an electronic Lieb lattice, Nat. Phys. **13**, 672 (2017).